CHEMISTRY

Electronic landscape of the *f*-electron intermetallics with the $ThCr_2Si_2$ structure

You Lai[1,2], Julia Y. Chan[3], Ryan E. Baumbach[1,2]*

Although strongly correlated *f*-electron systems are well known as reservoirs for quantum phenomena, a persistent challenge is to design specific states. What is often missing are simple ways to determine whether a given compound can be expected to exhibit certain behaviors and what tuning vector(s) would be useful to select the ground state. In this review, we address this question by aggregating information about Ce, Eu, Yb, and U compounds with the $ThCr_2Si_2$ structure. We construct electronic/magnetic state maps that are parameterized in terms of unit cell volumes and *d*-shell filling, which reveals useful trends including that (i) the magnetic and nonmagnetic examples are well separated, and (ii) the crossover regions harbor the examples with exotic states. These insights are used to propose structural/chemical regions of interest in these and related materials, with the goal of accelerating discovery of the next generation of *f*-electron quantum materials.

INTRODUCTION

Interest in strongly correlated *f*-electron intermetallics is periodically renewed by discoveries of exemplary materials with remarkable behaviors [e.g., hidden order and superconductivity in URu_2Si_2 (*1*), anomalously high temperature superconductivity in $PuCoGa_5$ (*2*), topological insulating behavior in SmB_6 (*3*), strongly correlated Weyl-Kondo semimetallic behavior in Ce-based compounds (*4*), and heavy fermion superconductivity in many Ce- and U-based systems (*5*, *6*)]. The vitality of this cycle was recently seen in the emergence of unconventional spin triplet superconductivity in UTe_2 (*7*, *8*), which features anomalously large upper critical fields and magnetic field–driven reentrant superconductivity. Even among the heavily studied variants of the $ThCr_2Si_2$ structure, this trend toward serendipitous discovery is alive and well. For example, $CeRh_2As_2$ ($CaBe_2Ge_2$-type structure) was recently shown to exhibit unconventional superconductivity, anomalously large upper critical fields, and evidence for several superconducting order parameters (*9*, *10*). Both of these materials may even feature nontrivial electronic topologies.

These types of discoveries clearly invite continued efforts to develop *f*-electron intermetallics, but the field is hampered by a lack of clarity regarding where to look for examples with enhanced properties. This is largely because (i) the relative strengths of interactions (e.g., Kondo, RKKY, valence instability, spin orbit, crystal electric field splitting, etc.) vary widely between different materials, (ii) unusual states often emerge as a result of finely balanced or cumulative interactions, and (iii) calculations to quantify the relative importance of different interactions often have limited success. Historically, this has necessitated systematic experimental surveys of the chemical/structural phase space to uncover materials with novel electronic and magnetic states (*11*). However, it is also widely held that these resource-intensive surveys are not optimal—at least in the sense that the discovery of examples with remarkable physics requires sifting through a large number of related examples.

What is often missing in this process is a simple way to determine whether a given compound can reasonably be expected to exhibit novel behavior (either intrinsically or under modest tuning) and what tuning vector(s) would be useful. Here, we address this challenge by reexamining the families of materials with the AT_2X_2 composition (*12*, *13*), where we show that for the *A* = Ce-, Eu-, Yb-, and U-based subsets with the $ThCr_2Si_2$-type structure, (i) the magnetic and nonmagnetic examples are well separated, (ii) the crossover region that separates them follows a simple but nontrivial trajectory, and (iii) the crossover region hosts the examples that exhibit attractive behavior such as unconventional superconductivity and non–Fermi liquid behavior. These observations are consistent with earlier organizing principles [e.g., the Doniach phase diagram (*14*), the Hill plot (*15*), and surveys of Ce- and U-based 122 compounds (*16*–*18*) that emphasize electronic hybridization strength] but have the benefit that they (i) clarify chemical strategies to search for new examples with novel behavior and (ii) provide a concise summary of behaviors in this structural family. We also suggest that this approach is well suited to elementary data mining of electronic databases that can be used to investigate many other structural families.

STRUCTURE, CHEMISTRY, AND GENERIC PHASE DIAGRAMS

The $ThCr_2Si_2$ structure (Fig. 1A) was first reported by Ban and Sikirica in (*12*), and since then, it has proven to be one of the most ubiquitous structural arrangements for ternary combinations of elements. There are many detailed reviews that address trends in this family, and several are listed in (*13*). To summarize, it is a ternary variant of the $BaAl_4$ prototype (space group *I*4/*mmm*) and is generically expressed as AT_2X_2, where the *A*, *T*, and *X* atoms are located on the Wyckoff sites 2*a* (0,0,0), 4*d* (0,0.5,0.25), and 4*e* (0,0,z), respectively. This provides distinct high-symmetry environments around the *A*, *T*, and *X* atoms that influence the physical properties of the chemical variants. This structure also exhibits pronounced chemical flexibility, where the *A* site can be populated by alkali metal, alkaline earth, rare earths, first column transition metals, lanthanide, and actinide elements; the *T* site can be occupied by transition metal, light alkali metals and alkaline earths, and *p*-block elements; and the *X* site can be occupied by *p*-block elements and some transition metals. There are many other closely related structures [e.g., $CaBe_2Ge_2$, $CeNiSi_2$, $BaNiSn_3$, and $U_2Co_3Si_5$ types (*19*–*22*)], and there are even hybrid examples that combine this family and other prototypes

[1]National High Magnetic Field Laboratory, Florida State University, Tallahassee, FL 32310, USA. [2]Department of Physics, Florida State University, Tallahassee, FL 32306, USA. [3]Baylor University, Waco, TX 76706, USA.
*Corresponding author. Email: baumbach@magnet.fsu.edu

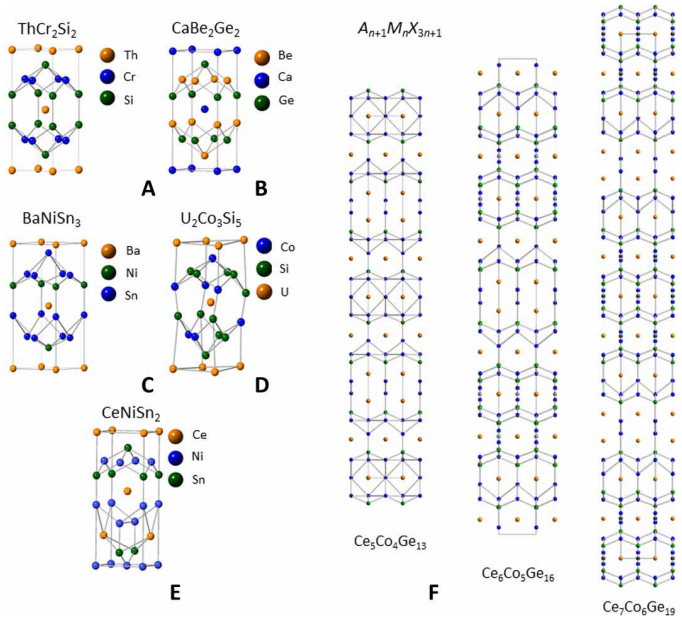

Fig. 1. Summary of crystalline structures that relate to the $ThCr_2Si_2$ prototype. (**A** to **E**) The $ThCr_2Si_2$, $CaBe_2Ge_2$, $BaNiSn_3$, $U_2Co_3Si_5$, and $CeNiSi_2$ structures taken from (*12*, *13*, *19*–*22*). (**F**) The structure for the $A_{n+1}M_nX_{3n+1}$ (A = lanthanide, M = transition metal, X = tetrels), n = 4 to 6 compounds, composed of complex layering of subunits. Ce, Co, and Ge are represented as orange, green, and blue spheres, respectively. Structural details obtained from (*23*–*25*).

(Fig. 1, B to F) (*23*–*25*), which opens the prospect of developing design principles that span families of materials.

A multitude of behaviors emerge from these simple crystal structures when *f*-elements are introduced into them, including local moment and complex magnetism (*26*), charge instabilities (*27*), structural instabilities (*28*), unconventional superconductivity (*29*, *30*), hidden order (*1*), multipolar order (*31*), and topologically protected electronic states (*9*, *10*). For the Ce-, Yb-, and U-based systems, the behavior is especially rich and is often understood in terms of the Ruderman-Kittel-Kasuya-Yosida (RKKY) and Kondo interactions (*14*, *32*–*35*), where (i) the RKKY interaction provides an indirect magnetic exchange between localized f-spins through the conduction electrons and favors magnetic ordering while (ii) the Kondo interaction drives hybridization between the conduction electron and *f*-states that results in screening of the *f*-spin and strongly reduces the effective magnetic moment. The connection between these parameters has been discussed extensively in terms of the Doniach model and is summarized in (*5*, *6*). The resulting generic phase diagrams are shown schematically in Fig. 2 (A and B) for Ce and Yb, where a tuning parameter δ (e.g., pressure or chemical substitution) varies the ground state. For the case of Ce, at small δ, the valence is close to 3+, hybridization between the *f*- and conduction electrons is weak, and there typically is a magnetically ordered ground state at $T_{N,C}$. As δ increases, $T_{N,C}$ may initially increase as the RKKY interaction strengthens, but eventually, it tends to be suppressed toward zero temperature at δ_c. Under some conditions, this results in a quantum critical point that is surrounded by a fan-like region of non–Fermi liquid behavior. For many CeT_2X_2 compounds, the quantum critical point is also surrounded by a dome of unconventional superconductivity. At larger δ, the hybridization strength increases further, Fermi liquid behavior is observed below a crossover temperature T_{FL}, and eventually intermediate valence or a tetravalent state emerges. The Ce and Yb phase diagrams are related but are inverted with respect to each other owing to how Hund's rules determine the total angular momentum J: for Ce^{3+} (J = 5/2) and Ce^{4+} (J = 0), and for Yb 2+ (J = 0) and Yb 3+ (J = 7/2).

Some lanthanide- and actinide-based materials with multiple *f*-orbitals exhibit related phase diagrams, but additional complexities are involved. For example, a semi-universal phase diagram has been proposed for Eu-based intermetallics (*36*, *37*), which resembles the Doniach picture but also includes distinct features relating to the valence transition between the Eu^{2+} (J = 7/2) and Eu^{3+} (J = 0) states (Fig. 2C). There is also an ongoing debate about the importance of valence instabilities in Ce- and Yb-based materials, their role in determining classes of quantum criticality, and impact on superconductivity (*38*–*40*). We point out that related behavior might even be expected in families containing Pr, Sm, and Tm where multiple valence states are available (*41*, *42*). Among actinide-based materials, the situation is even more complicated due to the greater tendency toward *f*-state itinerancy, the potential impact of relativistic effects, and the presence of multiple *f*-electron orbitals that could experience differing degrees of hybridization (*43*). Nonetheless, phase diagrams that resemble those shown in Fig. 2 (A to C) are sometimes observed (*44*, *45*). Last, all of these behaviors should be contrasted with those of the remaining lanthanides, where (i) the valence is rigidly fixed to be trivalent and (ii) hybridization between the conduction electron and *f*-states is weak.

On the basis of these observations, it is appealing to suggest that although there are wide-ranging behaviors in this family of materials, the QCP scenario provides a powerful design principle for producing examples with attractive behaviors. However, even with these insights, it remains unclear (i) which ones are best suited to further investigations because they are near a magnetic or valence instability and (ii) for a given material (or family of materials) what is the best tuning strategy to access regions of interest. To address this, we assemble maps in the chemical-structural phase space for the compounds $(Ce,Yb,Eu,U)T_2X_2$ with the $ThCr_2Si_2$ structure and identify regions of interest. We also comment on related structures and prospects for uncovering novel phenomena in them.

ELECTRONIC-MAGNETIC MAPS FOR $(Ce,Yb,Eu,U)T_2X_2$ WITH THE $ThCr_2Si_2$ STRUCTURE

Figure 3A presents the phase map for the compounds CeT_2X_2 (T = transition metal and X = Si, Ge) by providing the lattice constants and *f*-state as reported in literature (*16*–*18*, *29*, *40*, *46*–*77*). By organizing these compounds based on their transition metal column and unit cell volume, it is seen that (i) there is a clear separation between those with trivalent Ce and tetravalent or intermediate valence Ce; (ii) the crossover region includes all of the examples that exhibit Kondo lattice heavy fermion, quantum criticality, non–Fermi liquid, and superconducting behavior; and (iii) the crossover region depends on a nearly linear relationship between shell filling and unit cell volume. Points (i) and (ii) are illustrated by the evolution from a strongly hybridized Kondo lattice ($CeCu_2Si_2$) toward weakened hybridization and strengthened magnetism as the unit cell volume increases (*29*). This is also noticeable for the other isovalent transition metal series, which all go from tetravalent examples [e.g., $CeNi_2Si_2$ (*61*)] through strongly hybridized Kondo lattices

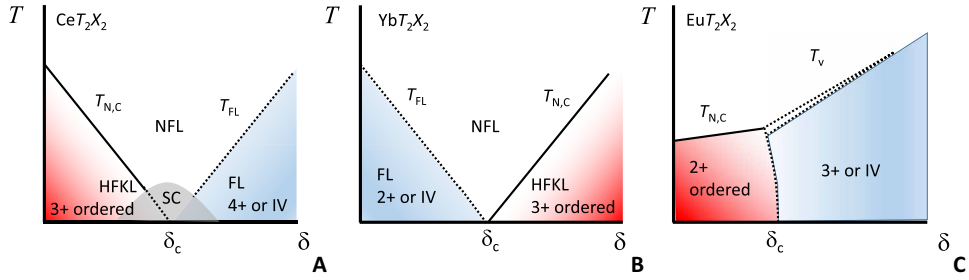

Fig. 2. Schematic phase diagrams for strongly correlated *f*-electron intermetallics. Temperature T versus control parameter δ phase diagram for the compounds (**A**) CeT_2X_2 (*5*, *6*), (**B**) YbT_2X_2 (*5*, *6*), and (**C**) EuT_2X_2 (*36*, *37*), where T = transition metal and X = *p*-block element. Here, δ is the chemical composition x or pressure P. The trends for the magnetic ordering temperatures $T_{N,C}$, superconducting transition temperatures T_c, valence change transition temperatures T_V, and Fermi liquid crossovers T_{FL} that are observed in these phase diagrams are described in the text. The solid lines represent phase boundaries, whereas the dotted lines represent crossover regions: e.g., temperature ranges over which a system enters a Fermi liquid or intermediate valence (IV) ground state. The *f*-electron valences are also indicated (3+ or 4+ for cerium, 2+ or 3+ for ytterbium, and 2+ or 3+ for europium). Note that these diagrams focus on the critical regions near δ_c, but the more general Doniach phase diagram includes a region where the ordering temperatures increase with δ as the RKKY interaction strengthens, before collapsing toward $T = 0$ at δ_c (*14*). This trend is seen in the ordering temperatures presented in Fig. 3.

[e.g., $CeNi_2Ge_2$ (*60*, *61*)] to trivalent cerium magnetism [$CePd_2Ge_2$ (*59*, *60*)]. Supporting evidence for this evolution is seen by examining the unit cell volume lanthanide contractions for each family of materials, where reductions from the trivalent lanthanide contraction are seen for tetravalent or intermediate valence examples. Related behavior is observed for many other cerium-based intermetallics and is generally understood in the context of the Doniach picture or in terms of empirical frameworks such as Hill plots (Fig. 2A) (*6*, *14*, *15*).

The effect of non-isoelectronic tuning is less easily anticipated but is clarified by earlier studies showing that the hybridization strength between the *f*-electron and conduction electron states tends to decrease going from the iron column toward the copper column (*16*–*18*). Within the Ce-map, the importance of this is seen for the group of materials with unit cell volumes near 170 $Å^3$, where there is a progression from intermediate valence or tetravalent behavior [$CeOs_2Si_2$ (*51*)] to heavy fermion Kondo lattice behavior [$CeIr_2Si_2$ (*56*)], to quantum-critical non–Fermi liquid behavior and superconductivity [$CeNi_2Ge_2$ (*60*, *61*)], and lastly trivalent magnetic ordering [$CeCu_2(Si_{1-x}Ge_x)_2$ at $x \approx 0.2$ (*66*)]. This illustrates that weakening hybridization causes the boundary between magnetic (Ce^{3+}) and nonmagnetic (Ce^{4+} or intermediate valence) behavior to shift toward smaller unit cell volumes with increasing *d*-shell filling. Outside of this crossover region, horizontal lines always traverse either intermediate valence or tetravalent cerium states (small volumes) or trivalent cerium states with magnetic ordering (large volumes).

The examples that exhibit heavy Fermi liquid Kondo lattice behavior, superconductivity, or non–Fermi liquid behavior [e.g., $CeRu_2Si_2$ (*50*), $CeCu_2Si_2$ (*29*), and $CeNi_2Ge_2$ (*60*, *61*)] appear at the boundary between the two regions and are readily tuned through it by changing either the unit cell volume or the *d*-shell filling. For example, in the cases of $CeCu_2Si_2$ and $CeNi_2Ge_2$, applied pressure drives the ambient pressure superconducting transition through a dome-like region (*29*, *60*). Fermi liquid behavior that is consistent with the system entering either an intermediate valence or tetravalent cerium state emerges at large pressures, where a second dome of superconductivity is observed. In contrast, isoelectronic chemical substitution that expands the lattice drives these compounds into magnetic ground states where the hybridization strength is reduced. It is also seen that the examples with magnetically ordered ground states that are near the boundary [e.g., $CePd_2Si_2$ (*60*) and $CeRh_2Si_2$ (*54*)] are readily moved into it using applied pressure, while larger pressures are needed to move more distant examples [e.g., $CeAu_2Si_2$ (*40*) and $CeCu_2Ge_2$ (*67*)] into the crossover region. Non-isoelectronic chemical substitution series reveal related trends: e.g., when antiferromagnetic $Ce(Cu_{1-x}T_x)_2Ge_2$ ($x = 0$) is chemically substituted by T = Ni or Co, the boundary region is crossed and critical behavior is observed over a limited x-range (*47*, *69*).

Thus, it is clear that for the entire $CeT_2(Si,Ge)_2$ series, the region that separates the magnetic and nonmagnetic members varies systematically with both the unit cell volume and the electronic shell filling, each tuning the hybridization strength in a distinct way. This perspective is reinforced by considering the related maps for the compounds CeT_2X_2 (T = transition metal and X = P, As; Fig. 3B) (*70*–*77*). Although it is less clear in this case, we infer from these data and the trends that are seen for the Si/Ge analogs that there is a similar non-trivial vector separating the magnetic and nonmagnetic regions. As before, the examples that exhibit strongly correlated electron physics [e.g., $CeRu_2P_2$ (*71*)] are on the boundary.

Given the success of this simple scheme in describing the Ce-based $ThCr_2Si_2$ compounds, we next examine the maps for the Yb examples (Fig. 4) (*30*, *31*, *78*–*97*). Note that few pnictide analogs have been reported, so a map is not included. For the Si/Ge series, there is a strong resemblance between the Yb and Ce maps, but the magnetic and nonmagnetic regions are inverted. This is due to Hund's rules producing $J = 7/2$ for trivalent ytterbium ($4f^{13}$), while divalent Yb has a full *f*-shell ($4f^{14}$ and $J = 0$). In the intermediate volume region, there are several nearly critical Kondo lattice systems, as well as the well-known quantum critical material $YbRh_2Si_2$ (*30*, *84*). Chemical substitution studies have been performed for many of these examples: e.g., (i) Rh → Co substitution in $YbRh_2Si_2$ stabilizes magnetism, weakens the hybridization strength, and leads to magnetic ordering (*97*); (ii) applied pressure drives $YbFe_2Ge_2$ from being a heavy fermion Kondo lattice through a quantum critical point with non–Fermi liquid behavior, into an antiferromagnetically ordered ground state (*80*); and (iii) applied pressure drives divalent $YbCu_2Ge_2$ toward intermediate valence behavior (*94*). Similar behavior is seen for tuning studies of other examples such as $YbIr_2Si_2$ (*83*), $YbCu_2Si_2$ (*95*), and $YbPd_2Si_2$ (*96*). These observations suggest that the hybridization strength for the Yb compounds is strongly

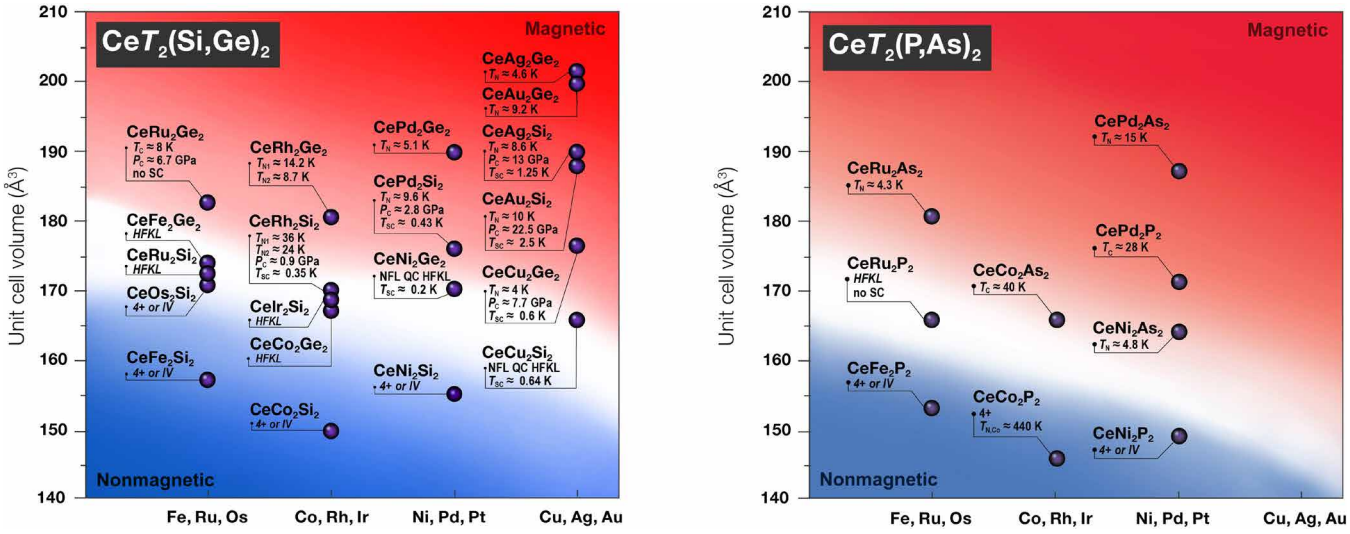

Fig. 3. Phase map for the valence and ground state behavior of the compounds CeT_2X_2 (T = transition metal and X = Si/Ge and P/As) that crystallize in the $ThCr_2Si_2$-type structure (*16–18, 29, 40, 46–77*). The axes that control the ground state are the unit cell volume (V) and the d-shell filling going from the Cu column to the Fe column. The white band that traverses the center of the phase diagram is a guide to the eye that approximately separates the examples with tetravalent or intermediate valence cerium [lower left-hand side (blue background)] from those with trivalent cerium [upper right-hand side (red background)]. Ordering temperatures are labeled (Neel temperature T_N and Curie temperature T_C). Also shown in some cases are the critical pressures where magnetism collapses (P_c) and the associated superconducting transition temperature (T_c). These values and their associated references are summarized in table S1.

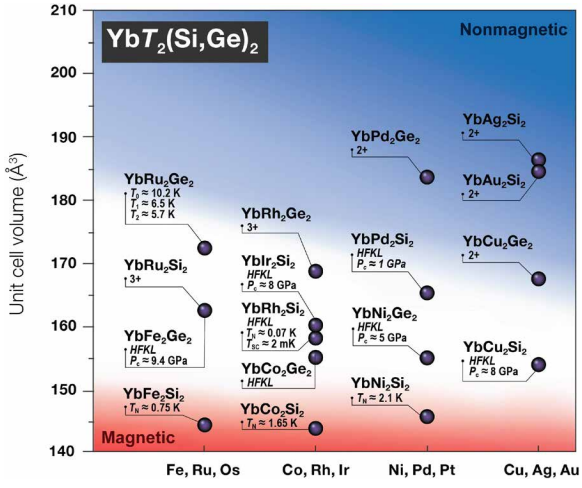

Fig. 4. Phase map for the valence and ground state behavior of the compounds YbT_2X_2 (T = transition metal and X = Si/Ge) that crystallize in the $ThCr_2Si_2$-type structure (*30, 31, 78–97*). The white band that traverses the center of the phase diagram is a guide to the eye that approximately separates the examples with trivalent [bottom (red background)] from those with divalent ytterbium [upper right-hand side (blue background)]. Ordering temperatures are labeled (Neel temperature T_N and Curie temperature T_C). Critical pressures P_c are labeled. These values and their associated references are summarized in table S2.

controlled by a combination of lattice contraction and d-shell filling in a manner that resembles what is seen for the Ce analogs.

It is also of interest to examine other Pr-, Sm-, Eu-, and Tm-based compounds that potentially could exhibit valence instabilities (*41*, *42*). Among this group, those with Pr, Sm, and Tm so far show no evidence in their bulk properties for crossover regions. This is supported by inspection of the evolution of their unit cell volumes, where all examples conform to the trivalent lanthanide contraction. This leads us to expect that although these families might, in principle, include interface regions, they are not within the chemical phase space of the naturally occurring examples in this structure.

In contrast, the Eu compounds show trends that are related to the Ce and Yb analogs (Fig. 5) (*36*, *37*, *98–131*). The compressed volume examples all exhibit either trivalent ($4f^6$, $J = 0$) or intermediate valence behavior while the expanded volume examples exhibit divalent ($4f^7$, $J = 7/2$) behavior. Examples close to the crossover region are readily tuned through it: e.g., the Eu valence and unit cell volume of $EuCu_2Si_2$ vary between 2+ and 3+ depending on synthesis method (*115*, *116*) while $EuIr_2Si_2$ exhibits behavior that is similar to what is seen in Kondo lattice systems with modest hybridization strength (*104*). When the antiferromagnets $EuNi_2Ge_2$ (*108*) and $EuRh_2Si_2$ (*102*) are compressed using hydrostatic pressure, they evolve toward Kondo lattice–like behavior similar to that of $EuIr_2Si_2$. Remarkable behavior is seen for $EuPd_2Si_2$, which is nearly divalent at room temperature but its temperature-dependent volume contraction is sufficient to drive a phase transition into the trivalent state (*36*, *107*). Among the pnictides, it is noteworthy that although most of them exhibit a divalent state, the heavy fermion Kondo lattice $EuNi_2P_2$ appears to be in a crossover region where the critical unit cell volume is substantially smaller than that of the Si/Ge analogs (*130*, *131*). These maps also reveal an important distinction from the Ce and Yb analogs, since here the electronic shell filling has a negligible impact on the location of the crossover region.

Last, Fig. 6 summarizes results for the compounds UT_2X_2 (*1*, *79*, *132–146*). There are a limited number of pnictide examples, so we focus on the Si/Ge group. Again, there is a separation between the magnetic and nonmagnetic examples, but in this case, the latter group is clustered around the Fe/Ru/Os transition metal group. Most of these compounds are Pauli paramagnets [e.g., UFe_2Si_2 (*134*), UFe_2Ge_2 (*133*), and UOs_2Si_2 (*132*)] where strong hybridization between the

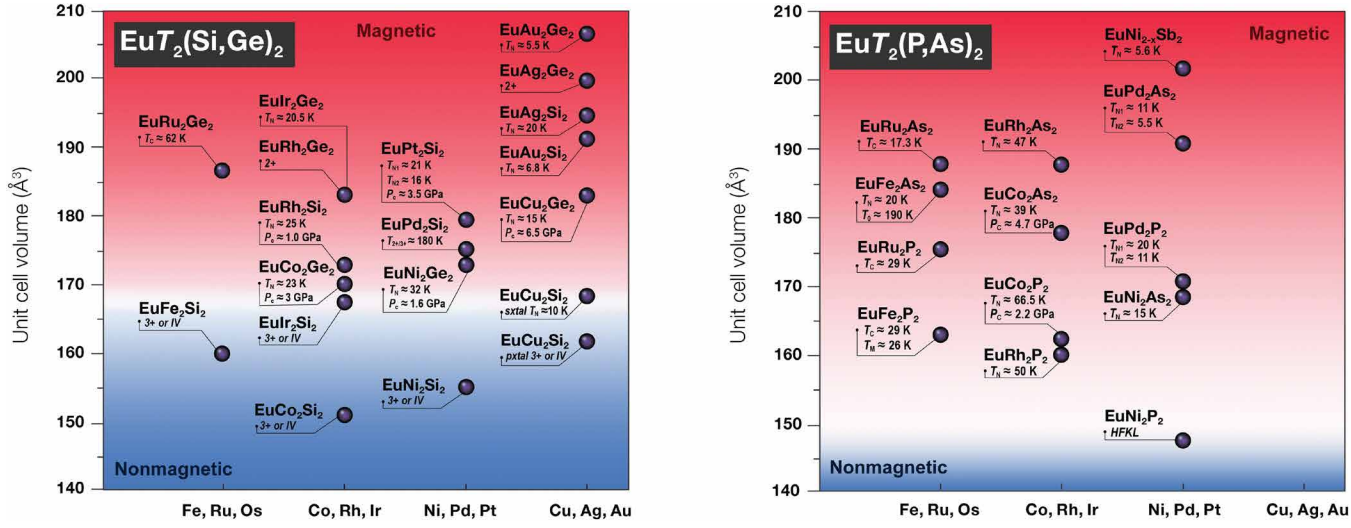

Fig. 5. Phase map for the valence and ground state behavior of the compounds EuT_2X_2 (T = transition metal and X = Si/Ge and P/As) that crystallize in the $ThCr_2Si_2$-type structure (*36*, *37*, *98*–*131*). The white band that traverses the center of the phase diagram is a guide to the eye that separates the examples with trivalent or intermediate valence europium [lower half (blue background)] from those with divalent europium [upper half (red background)]. Ordering temperatures are labeled (Neel temperature T_N and Curie temperature T_C). Critical pressures P_c are labeled. These values and their associated references are summarized in table S3.

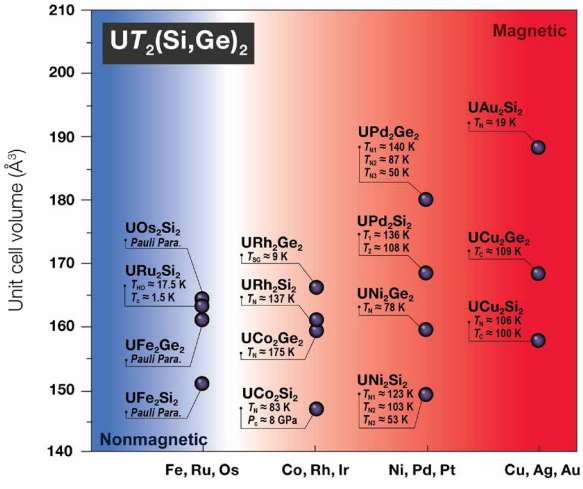

Fig. 6. Phase map for the valence and ground state behavior of the compounds UT_2X_2 (T = transition metal and X = Si/Ge) that crystallize in the $ThCr_2Si_2$-type structure (*1*, *79*, *132*–*146*). The white band separates the examples with Pauli paramagnetism [left-hand side (blue background)] from those with magnetically ordered ground states [right-hand side (red background)] is a guide to the eye. Ordering temperatures are labeled (Neel temperature T_N, Curie temperature T_C, hidden order temperature T_{HO}, spin glass temperature T_{sg}, and superconducting transition temperature T_c). Critical pressures P_c are labeled. These values and their associated references are summarized in table S4.

f- and conduction electron states causes the *f*-state to become delocalized. It is interesting to note that the hidden order compound, URu_2Si_2, is located in close vicinity to these examples, which is consistent with the view that strong hybridization plays an important role in this material (*1*). Similar to what is seen for the lanthanides, the hybridization strength weakens going toward the Cu/Ag/Au column (*16*, *17*). The result is that the remainder of the compounds all exhibit magnetic ground states with large ordering temperatures. Some of these examples host complex magnetism [e.g., spin glass behavior in URh_2Ge_2 (*135*) and multiple phase transitions in many others] and are susceptible to disorder effects, but these behaviors do not appear to be associated with the crossover region. Decreases in the unit cell volume tend to slowly suppress the ordering temperature, but in contrast to the Ce, Yb, and Eu analogs, there is no volume-driven crossover region for this family. Instead, large pressures are needed to access it, as demonstrated for UCo_2Si_2 that has a critical pressure near 8 GPa (*140*). For UNi_2Si_2 and UCu_2Si_2, even larger pressures would be needed, as experiments have so far been unsuccessful in fully suppressing the magnetism (*141*, *146*). Thus, it is clear that the U series is distinct from the Ce, Yb, and Eu analogs in terms of the conditions that would be useful for driving critical behavior. This has been remarked upon previously (*146*) and likely reflects differences between the 5*f* and 4*f* states. Such information is of high importance in developing tuning strategies to access the critical region.

OUTLOOK FOR FUTURE EFFORTS

These insights are immediately useful for focusing investigations of materials with the $ThCr_2Si_2$ structure. For example, although the Ce-series has already been extensively studied, there remain some attractive examples that have not received close attention. $CeCo_2As_2$ (*73*) is of interest because it is simultaneously near the crossover region and may also exhibit strong *d*-electron magnetism similar to what is seen for $CeCo_2P_2$ (*74*). Preliminary results reveal ferromagnetic ordering at $T_C \approx 40$ K (*73*), and we speculate that the ordered state would be readily suppressed using applied pressure, As → P substitution, or Co → Fe or Ni substitution. Examination of the Eu and Yb families reveals other opportunities. Both $EuFe_2Ge_2$ and $EuRu_2Si_2$ have not been reported, although the related compounds RFe_2Ge_2 (R = Y, Pr, Nd, Sm, Gd-Tm, and Lu) and EuT_2Ge_2 (T = transition metal) are described in (*147*, *148*). Here, it was inferred that $EuFe_2Ge_2$ is not a stable phase under conventional growth conditions. This

leads us to propose that this phase, and others that are "missing" from the maps, might be accessible as metastable phases where modest amounts of applied or chemical pressure might be sufficient to stabilize them. If they can be formed, they might exhibit complex phase diagrams involving valence instability physics similar to what is seen in $EuPd_2Si_2$ (*36*, *107*), $EuRh_2Si_2$ (*102*), or $EuCo_2Ge_2$ (*103*), where modest lattice contractions are sufficient to access the valence change region. The heavy fermion Kondo lattice $EuNi_2P_2$ appears to be within the crossover region and exhibits Kondo lattice–like behavior (*130*, *131*). This invites efforts to traverse the crossover region using chemical substitution. Last, for the Yb-based examples, we note that there have already been substantial efforts, where the focus has been on the prototypical quantum critical point material $YbRh_2Si_2$ (*30*, *84*). Nonetheless, there are several other remarkable materials in this family including $YbRu_2Ge_2$ (*31*), which exhibits quadrupolar order and strongly correlated electron behavior. This is unique among all other lanthanide-based materials with the $ThCr_2Si_2$ structure and motivates chemical substitution studies that span the crossover region.

The U-based examples show distinct trends that draw attention toward *d*-shell filling as being the only viable route for entering the crossover region. This perspective has already been explored for URu_2Si_2 (*149*, *150*), where electronic shell filling produces a semi-universal *T*-*x* phase diagram with three main regions: (i) The hidden order state is rapidly suppressed toward zero temperature for $x \lesssim x_{cr,1}$, (ii) paramagnetism with a heavy–Fermi liquid ground state is seen for $x_{cr,1} \lesssim x \lesssim x_{cr,2}$, and (iii) complex antiferromagnetic order appears for $x_{cr,2} \lesssim x$. Unexpectedly, this behavior is induced regardless of the type of chemical substitution (e.g., Ru → Rh, Ir, and Si → P), as long as it effectively adds electrons. This motivates further studies of the nearby Pauli paramagnetic analogs, where non-isoelectronic chemical substitution can be used to tune toward the magnetic region [e.g., $U(Fe_{1-x}T_x)_2Ge_2$, where *T* = Co, Rh, and Ir].

Last, it will be valuable to use these insights to cast a wider net into the structural variants with the $CaBe_2Ge_2$, $CeNiSi_2$, $BaNiSn_3$, and $U_2Co_3Si_5$ structure types, where a preliminary survey indicates that they exhibit maps that are similar to those presented here. Recent work has also shown that there are complex hybrid structures that combine standard building blocks with other structural elements. An example of this is seen for the homologous series $A_{n+1}M_nX_{3n+1}$ (*A* = lanthanide, *M* = transition metal, *X* = tetrels, and *n* = 1 to 6), which are constructed from basic structural subunits such as AlB_2, $AuCu_3$, and $BaNiSn_3$ (Fig. 1F). Examples spanning *n* = 1 to 6 for the *A* = Ce series have already been uncovered (*23*–*25*), where complex magnetism and Kondo lattice physics is observed. For example, $Ce_7Co_{6+x}Ge_{19-y}Sn_y$ (*n* = 6), with four crystallographically unique lanthanide sites, was recently shown to have five magnetic transitions of 5, 6, 7.2, 12.4, and 16.5 K. It was also shown that three of the *n* = 6 magnetic transitions are also found in the *n* = 5 member (*24*). This opens the possibility that magnetic/electronic behaviors can be controlled using varied stacking arrangements. The diversity of this behavior invites further investigations, where we expect (i) additional *n* variation and (ii) chemical flexibility on all of the crystallographic sites. It is easy to look forward to (i) the Eu, Yb, and U analogs being hosts for many different novel electronic/magnetic behaviors and (ii) the transition metal and tetrel sites accomodating isoelectronic replacement and possibly even nonisoelectronic substitution. While a brute force examination of the chemical phase space is not feasible, our maps offer a route forward. For example, all of the Ce-based examples that have been uncovered so far exhibit local *f*-moment magnetism. Taking inspiration from the maps for the $ThCr_2Si_2$ Ce-based materials, this implies that efforts should be made to increase the hybridization strength by compressing the unit cell volume (e.g., using applied pressure or Ge → Si substitution) and undertaking chemical substitution studies that point toward the iron column.

SUMMARY AND CONCLUSION

In this review, we have constructed structural/chemical maps for intermetallics with the $ThCr_2Si_2$ structure, which reveal distinct regions where classes of *f*-state behaviors emerge. In particular, among the Ce, Eu, Yb, and U families, the cases with magnetic *f*-states are separated from those with strongly hybridized nonmagnetic *f*-states by a well-contained crossover region that depends on both unit cell volume and electron shell filling. The examples that exhibit emergent behavior that is associated with quantum criticality are found in the crossover region. This agrees with earlier perspectives (e.g., Doniach and Hill) but clarifies the role of chemical composition without resorting to computational methods. These insights will be useful to pinpoint regions of interest in families of materials related to the $ThCr_2Si_2$ prototype and have the potential to accelerate discoveries of intriguing phenomena. This approach may even be applicable to other structural families, where mining of electronic databases could be used to accelerate progress.

SUPPLEMENTARY MATERIALS

Supplementary material for this article is available at https://science.org/doi/10.1126/sciadv.abp8264

REFERENCES AND NOTES

1. J. A. Mydosh, P. M. Oppeneer, P. S. Riseborough, Hidden order and beyond: An experimental-theoretical overview of the multifaceted behavior of URu_2Si_2. *J. Phys. Condens. Matter* **32**, 143002 (2020).
2. J. L. Sarrao, L. A. Morales, J. D. Thompson, B. L. Scott, G. R. Stewart, F. Wastin, J. Rebizant, P. Boulet, E. Colineau, G. H. Lander, Plutonium based superconductivity with a transition temperature above 18 K. *Nature* **420**, 297–299 (2002).
3. M. Dzero, K. Sun, V. Galitski, P. Coleman, Topological Kondo insulators. *Phys. Rev. Lett.* **104**, 106408 (2010).
4. H.-H. Lai, S. E. Grefe, S. Paschen, Q. Si, Weyl–Kondo semimetal in heavy-fermion systems. *Proc. Natl. Acad. Sci. U.S.A.* **115**, 93–97 (2018).
5. C. Pfleiderer, Superconducting phases *f*-electron compounds. *Rev. Mod. Phys.* **81**, 1551–1624 (2009).
6. M. B. Maple, R. E. Baumbach, N. P. Butch, J. J. Hamlin, M. Janoschek, Non-fermi liquid regimes and superconductivity in the low temperature phase diagrams of strongly correlated *d*- and *f*-electron materials. *J. Low Temp. Phys.* **161**, 4–54 (2010).
7. S. Ran, C. Eckberg, Q.-P. Ding, Y. Furukawa, T. Metz, S. R. Saha, I.-L. Liu, M. Zic, H. Kim, J. Paglione, N. P. Butch, Nearly ferromagnetic spin-triplet superconductivity. *Science* **365**, 684–687 (2019).
8. S. Ran, I.-L. Liu, Y. S. Eo, D. J. Campbell, P. M. Neves, W. T. Fuhrman, S. R. Saha, C. Eckberg, H. Kim, D. Graf, F. Balakirev, J. Singleton, J. Paglione, N. P. Butch, Extreme magnetic field-boosted superconductivity. *Nat. Phys.* **15**, 1250–1254 (2019).
9. S. Khim, J. F. Landaeta, J. Banda, N. Bannor, M. Brando, P. M. R. Brydon, D. Hafner, R. Küchler, R. Cardoso-Gil, U. Stockert, A. P. Mackenzie, D. F. Agterberg, C. Geibel, E. Hassinger, Field-induced transition within the superconducting state of $CeRh_2As_2$. *Science* **373**, 1012–1016 (2021).
10. K. Nogaki, A. Daido, J. Ishizuka, Y. Yanase, Topological crystalline superconductivity in locally noncentrosymmetric $CeRh_2As_2$. *Phys. Rev. Res.* **3**, L032071 (2021).
11. P. C. Canfield, New materials physics. *Rep. Prog. Phys.* **83**, 016501 (2019).
12. Z. Ban, M. Sikirica, The crystal structure of ternary silicides ThM_2Si_2 (*M* = Cr, Mn, Fe, Co, Ni, and Cu). *Acta Crystallogr.* **18**, 594–599 (1965).
13. M. Shatruk, $ThCr_2Si_2$ structure type: The "Perovskite" of intermetallics. *J. Solid State Chem.* **272**, 198–209 (2019).
14. S. Doniach, The Kondo lattice and weak antiferromagnetism. *Physica B+C* **91**, 231–234 (1977).

15. H. H. Hill. *Plutonium in 1970 and other Actinides*, W. N. Miner, Ed. (AIME, New York, 1970), p. 2.
16. T. Endstra, G. J. Nieuwenhuys, J. A. Mydosh, Hybridization model for the magnetic-ordering behavior of uranium- and cerium-based 1:2:2 intermetallic compounds. *Phys. Rev. B Condens. Matter* **48**, 9595–9605 (1993).
17. T. T. M. Palstra, A. A. Menovsky, G. J. Nieuwenhuys, J. A. Mydosh, Magnetic properties of the ternary compounds CeT_2Si_2 and UT_2Si_2. *J. Magn. Magn. Mater.* **54–57**, 435–436 (1986).
18. R. A. Neifeld, M. Croft, T. Mihalisin, C. U. Segre, M. Madigan, M. S. Torikachvili, M. B. Maple, L. E. DeLong, Chemical environment and Ce valence: Global trends in transition-metal compounds. *Phys. Rev. B Condens. Matter* **32**, 6928–6931 (1985).
19. B. Eisenmann, N. May, W. Müller, H. Schäfer, Eine neue strukturelle variante des $BaAl_4$-Typs: Der $CaBe_2Ge_2$-Typ. *Z. Naturforsch. B* **27**, 1155–1157 (1972).
20. W. Dörrscheidt, H. Schäfer, Die Struktur des $BaPtSn_3$, $BaNiSn_3$ und $SrNiSn_3$ und ihre Verwandtschaft zum $ThCr_2Si_2$-Strukturtyp. *J. Less Common Met.* **58**, 209–216 (1978).
21. O. I. Bodak, E. I. Gladyshevskii, System cerium-nickel-silicon in the region of 0-33 at. % Ce. *Inorg. Mater.* **5**, 1754–1758 (1969).
22. L. G. Akselrud, Y. P. Yarmolyuk, E. I. Gladyshevskii, Crystal structure of the compound $U_2Co_3Si_5$. *Sov. Phys. Crystallogt.* **22**, 492–493 (1977).
23. J. B. Felder, A. Weiland, H. Hodovanets, G. T. McCandless, T. G. Estrada, T. J. Martin, A. V. Walker, J. Paglione, J. Y. Chan, Law and disorder: Special stacking units—Building the intergrowth $Ce_6Co_5Ge_{16}$. *Inorg. Mater.* **58**, 6037–6043 (2019).
24. A. Weiland, K. Wei, G. T. McCandless, J. B. Felder, L. J. Eddy, R. E. Baumbach, J. Y. Chan, Strongly correlated electron behavior in a new member of the $A_{n+1}B_nX_{3n+1}$ homologous series:$Ce_7Co_6Ge_{19}$. *Phys. Rev. Mater.* **4**, 074408 (2020).
25. A. Weiland, K. Wei, G. T. McCandless, R. E. Baumbach, J. Y. Chan, Fantastic n= 4: $Ce_5Co_{4+x}Ge_{13-y}Sn_y$ of the $A_{n+1}M_nX_{3n+1}$ homologous series. *J. Chem. Phys.* **154**, 114707 (2021).
26. N. D. Khanh, T. Nakajima, X. Yu, S. Gao, K. Shibata, M. Hirschberger, Y. Yamasaki, H. Sagayama, H. Nakao, L. Peng, K. Nakajima, R. Takagi, T. Arima, Y. Tokura, S. Seki, Nanometric square skyrmion lattice in a centrosymmetric tetragonal magnet. *Nat. Nanotechnol.* **15**, 444–449 (2020).
27. J. Lee, K. Prokes, S. Park, I. Zaliznyak, S. Dissanayake, M. Matsuda, M. Frontzek, S. Stoupin, G. L. Chappell, R. E. Baumbach, C. Park, J. A. Mydosh, G. E. Granroth, J. P. C. Ruff, Charge density wave with anomalous temperature dependence in UPt_2Si_2. *Phys. Rev. B* **102**, 041112 (2020).
28. Y. Lai, K. Wei, G. Chappell, J. Diaz, T. Siegrist, P. J. W. Moll, D. Graf, R. E. Baumbach, Tuning the structural and antiferromagnetic phase transitions in UCr_2Si_2: Hydrostatic pressure and chemical substitution. *Phys. Rev. Mater.* **4**, 075003 (2020).
29. H. Q. Yuan, F. M. Grosche, M. Deppe, C. Geibel, G. Sparn, F. Steglich, Observation of two distinct superconducting phases in $CeCu_2Si_2$. *Science* **302**, 2104–2107 (2003).
30. E. Schuberth, M. Tippmann, L. Steinke, S. Lausberg, A. Steppke, M. Brando, C. Krellner, C. Geibel, R. Yu, Q. Si, F. Steglich, Emergence of superconductivity in the canonical heavy-electron metal $YbRh_2Si_2$. *Science* **351**, 485–488 (2016).
31. H. S. Jeevan, C. Geibel, Z. Hossain, Quasiquartet crystal-electric-field ground state with possible quadrupolar ordering in the tetragonal compound $YbRu_2Ge_2$. *Phys. Rev. B* **73**, 20407 (2006).
32. M. A. Ruderman, C. Kittel, Indirect exchange coupling of nuclear magnetic moments by conduction electrons. *Phys. Rev.* **96**, 99–102 (1954).
33. T. Kasuya, A theory of metallic ferro- and antiferromagnetism on Zener's model. *Prog. Theor. Exp. Phys.* **16**, 45–57 (1956).
34. K. Yosida, Magnetic properties of Cu-Mn alloys. *Phys. Rev.* **106**, 893–898 (1957).
35. J. Kondo, Resistance minimum in dilute magnetic alloys. *Prog. Theor. Exp. Phys.* **32**, 37–49 (1964).
36. C. U. Segre, M. Croft, J. A. Hodges, V. Murgai, L. C. Gupta, B. D. Parks, Valence instability in $Eu(Pd_{1-x}Au_x)_2Si_2$: The global phase diagram. *Phys. Rev. Lett.* **49**, 1947–1950 (1982).
37. Y. Ōnuki, M. Hedo, F. Honda, Unique electronic states of Eu-based compounds. *Journal of the Physical Society of Japan* **89**, 102001 (2020).
38. Y. Komijani, P. Coleman, Emergent critical charge fluctuations at the Kondo breakdown of heavy fermions. *Phys. Rev. Lett.* **122**, 217001 (2019).
39. L. Prochaska, X. Li, D. C. MacFarland, A. M. Andrews, M. Bonta, E. F. Bianco, S. Yazdi, W. Schrenk, H. Detz, A. Limbeck, Q. Si, E. Ringe, G. Strasser, J. Kono, S. Paschen, Singular charge fluctuations at a magnetic quantum critical point. *Science* **367**, 285–288 (2020).
40. Z. Ren, L. V. Pourovskii, G. Giriat, G. Lapertot, A. Georges, D. Jaccard, Giant overlap between the magnetic and superconducting phases of $CeAu_2Si_2$ under pressure. *Phys. Rev. X* **4**, 031055 (2014).
41. K. A. Gschneidner, L. Eyring, Eds., *Handbook on the Physics and Chemistry of Rare Earths, Volume 1: Metals* (North Holland Publishing Company, Amsterdam, 1978).
42. K. A. Gschneidner, L. Eyring, Eds., *Handbook on the Physics and Chemistry of Rare Earths, Volume 2: Alloys and Intermetallics* (North Holland Publishing Company, Amsterdam, 1979).
43. K. T. Moore, G. van der Laan, Nature of the 5*f* states in actinide metals. *Rev. Mod. Phys.* **81**, 235–298 (2009).
44. S. S. Saxena, P. Agarwal, K. Ahilan, F. M. Grosche, R. K. Haselwimmer, M. Steiner, E. Pugh, I. R. Walker, S. R. Julian, P. Monthoux, G. G. Lonzarich, A. D. Huxley, I. Sheikin, D. Braithwaite, J. Flouquet, Superconductivity on the border of itinerant-electron ferromagnetism in UGe_2. *Nature* **406**, 587–592 (2000).
45. T. C. Kobayashi, A. Hori, S. Fukushima, H. Hidaka, H. Kotegawa, T. Akazawa, K. Takeda, Y. Ohishi, E. Yamamoto, Pressure-temperature phase diagram and superconductivity in UIr. *J. Physical Soc. Japan* **76**, 051007 (2007).
46. K. A. Gschneidner, L. Eyring, Eds., *Handbook on the Physics and Chemistry of Rare Earths, Volume 12* (North Holland Publishing Company, Amsterdam, 1989).
47. E. V. Sampathkumaran, R. Vijayaraghavan, Evidence for 4*f*-ligand dehybridization in the evolution of heavy-fermion behavior in the series $CeCu_{2-x}Ni_xSi_2$. *Phys. Rev. Lett.* **56**, 2861 (1987).
48. S. Süllow, M. C. Aronson, B. D. Rainford, P. Haen, Doniach phase diagram, revisited: From ferromagnet to fermi liquid in pressurized $CeRu_2Ge_2$. *Phys. Rev. Lett.* **82**, 2963–2966 (1999).
49. M. B. Fontes, M. A. Continentino, S. L. Bud'ko, M. El-Massalami, L. C. Sampaio, A. P. Guimarães, E. Baggio-Saitovitch, M. F. Hundley, A. Lacerda, Physical properties of the $Ce(Ru_{1-x}Fe_x)_2Ge_2$ series. *Phys. Rev. B* **53**, 11678–11684 (1996).
50. L. C. Gupta, D. E. MacLaughlin, C. Tien, C. Godart, M. A. Edwards, R. D. Parks, Magnetic behavior of the Kondo-lattice system $CeRu_2Si_2$. *Phys. Rev. B* **28**, 3673–3676 (1983).
51. K. Hiebl, C. Horvath, P. Rogl, Magnetic behaviour of ternary silicides CeT_2Si_2 (T = Ru, Rh, Pd, Os, Ir, Pt) and boron substitution in $Ce(Ru,Os)_2Si_{2-x}B_x$. *J. Less Common Met.* **117**, 375–383 (1986).
52. M. Mihalik, V. Sechovsky, Electrical transport and magnetism in $CeFe_2Si_2$ single crystal. *Physica B* **359-361**, 163–165 (2005).
53. H. Abe, K. Yoshii, H. Kitazawa, Complex magnetic phase diagram of $CeRh_2Ge_2$. *Physica B* **312**, 253–255 (2002).
54. R. Movshovich, T. Graf, D. Mandrus, J. D. Thompson, J. L. Smith, Z. Fisk, Superconductivity in heavy-fermion $CeRh_2Si_2$. *Phys. Rev. B Condens. Matter* **53**, 8241–8244 (1996).
55. R. Settai, A. Misawa, S. Araki, M. Kosaki, K. Sugiyama, T. Takeuchi, K. Kindo, Y. Haga, E. Yamamoto, Y. Ōnuki, Single crystal growth and magnetic properties of $CeRh_2Si_2$. *J. Physical Soc. Japan* **66**, 2260–2263 (1997).
56. M. Mihalik, M. Diviš, V. Sechovský, Electronic and crystal structure of α- and β-$CeIr_2Si_2$. *Physica B* **404**, 3191–3194 (2009).
57. H. Fujii, E. Ueda, Y. Uwatoko, T. Shigeoka, Magnetic properties of $CeCo_2Ge_2$ and $NdCo_2Ge_2$ single crystals. *J. Magn. Magn. Mater.* **76**, 179–181 (1988).
58. B. Chevalier, J. Etourneau, J. Rossat-Mignod, R. Calemczuk, E. Bonjour, Evolution from the antiferromagnetic to the intermediate valence state in the $Ce(Rh_{1-x}Co_x)_2Si_2$ system. *J. Phys. Condens. Matter* **3**, 1847–1854 (1991).
59. H. Wilhelm, D. Jaccard, Calorimetric and transport investigations of $CePd_{2+x}Ge_{2-x}$ (x = 0 and 0.02) up to 22 GPa. *Phys. Rev. B* **66**, 064428 (2002).
60. F. M. Grosche, P. Agarwal, S. R. Julian, N. J. Wilson, R. K. W. Haselwimmer, S. J. S. Lister, N. D. Mathur, F. V. Carter, S. S. Saxena, G. G. Lonzarich, Anomalous low temperature states in $CeNi_2Ge_2$ and $CePd_2Si_2$. *J. Phys. Condens. Matter* **12**, L533–L540 (2000).
61. G. Knebel, M. Brando, J. Hemberger, M. Nicklas, W. Trinkl, A. Loidl, Magnetic, calorimetric, and transport properties of $Ce(Pd_{1-x}Ni_x)_2Ge_2$ and $CeNi_2(Ge_{1-y}Si_y)_2$. *Phys. Rev. B* **59**, 12390–12397 (1999).
62. A. Thamizhavel, R. Kulkarni, S. K. Dhar, Anisotropic magnetic properties of $CeAg_2Ge_2$ single crystals. *Phys. Rev. B* **75**, 144426 (2007).
63. C. L. Huang, V. Fritsch, W. Kittler, H. v. Löhneysen, Low-temperature properties of $CeAu_2Ge_2$ single crystals grown from Au-Ge and Sn flux. *Phys. Rev. B Condens. Matter* **86**, 214401 (2012).
64. C. S. Garde, J. Ray, Antiferromagnetism in $CeAu_2Si_2$- and $CeAg_2Si_2$-based Kondo-lattice systems. *J. Phys. Condens. Matter* **6**, 8585–8598 (1994).
65. G. W. Scheerer, Z. Ren, G. Lapertot, G. Garbarino, D. Jaccard, Heavy-fermion superconductivity in $CeAg_2Si_2$—Interplay of spin and valence fluctuations. *Physica B Condens. Matter* **536**, 150–154 (2018).
66. O. Trovarelli, M. Weiden, R. Müller-Reisener, M. Gómez-Berisso, P. Gegenwart, M. Deppe, C. Geibel, J. G. Sereni, F. Steglich, Evolution of magnetism and superconductivity in $CeCu_2(Si_{1-x}Ge_x)_2$. *Phys. Rev. B* **56**, 678–685 (1997).
67. D. Jaccard, K. Behnia, J. Sierro, Pressure induced heavy fermion superconductivity of $CeCu_2Ge_2$. *Phys. Lett. A* **163**, 475–480 (1992).
68. T. Ooshima, M. Ishikawa, Anomalous magnetic phase diagram of $Ce(Rh_{1-x}Co_x)_2Ge_2$. *J. Physical Soc. Japan* **67**, 3251–3255 (1998).
69. R. Tripathi, D. Das, C. Geibel, S. K. Dhar, Z. Hossain, Non-fermi-liquid behavior at the antiferromagnetic quantum critical point in the heavy-fermion system $Ce(Cu_{1-x}Cox)_2Ge_2$. *Phys. Rev. B* **98**, 165136 (2018).
70. K. Cheng, X. He, H. Yang, B. Zhou, Y. Li, Y. Luo, Synthesis and physical properties of $CeRu_2As_2$ and $CeIr_2As_2$. *Phys. Rev. B* **100**, 205121 (2019).
71. T. Fujiwara, K. Kanto, K. Matsubayashi, Y. Uwatoko, T. Shigeoka, Electrical transport properties of ternary phosphides RRu_2P_2 (R = La, Ce,Pr and Eu) with $ThCr_2Si_2$ type crystal structure. *J. Phys. Conf. Ser.* **273**, 012112 (2011).

72. M. Reehuis, W. Jeitschko, Structure and magnetic properties of the phosphides $CaCo_2P_2$ and LnT_2P_2 with $ThCr_2Si_2$ structure and LnTP with PbFCl structure (Ln = Lanthanoids, T = Fe, Co, Ni). *J. Phys. Chem. Solid* **51**, 961–968 (1990).
73. C. M. Thompson, "Magneto-Structural Correlations in Rare Earth-Cobalt Pnictides," thesis, The Florida State University (2012), vol. 74–02, 124 pp.
74. M. Reehuis, W. Jeitschko, G. Kotzyba, B. Zimmer, X. Hu, Antiferromagnetic order in the $ThCr_2Si_2$ type phosphides $CaCo_2P_2$ and $CeCo_2P_2$. *J. Alloys Compd.* **266**, 54–60 (1998).
75. T. Shang, Y. H. Chen, W. B. Jiang, Y. Chen, L. Jiao, J. L. Zhang, Z. F. Weng, X. Lu, H. Q. Yuan, Tunable magnetic orders in $CePd_2As_{2-x}P_x$. *J. Phys. Condens. Matter* **26**, 045601 (2014).
76. Y. Lai, S. E. Bone, S. Minasian, M. G. Ferrier, J. Lezama-Pacheco, V. Mocko, A. S. Ditter, S. A. Kozimor, G. T. Seidler, W. L. Nelson, Y.-C. Chiu, K. Huang, W. Potter, D. Graf, T. E. Albrecht-Schmitt, R. E. Baumbach, Ferromagnetic quantum critical point in $CePd_2P_2$ with Pd→Ni substitution. *Phys. Rev. B* **97**, 224406 (2018).
77. Y. Luo, J. Bao, C. Shen, J. Han, X. Yang, C. Lv, Y. Li, W. Jiao, B. Si, C. Feng, J. Dai, G. Cao, a. Zhu, Magnetism and crystalline electric field effect in $ThCr_2Si_2$-type $CeNi_2As_2$. *Physica B Condens. Matter* **86**, 245130 (2012).
78. A. Prasad, H. S. Jeevan, C. Geibel, Z. Hossain, Suppression of quadrupolar order on Si Doping in $YbRu_2(Ge_{1-x}Si_x)_2$. *J. Phys. Condens. Matter* **22**, 126004 (2010).
79. K. Hiebl, C. Horvath, P. Rogl, M. J. Sienko, Magnetic properties and structural chemistry of ternary silicides (RE,Th,U)Ru_2Si_2 (RE = rare earth). *J. Magn. Magn. Mater.* **37**, 287–296 (1983).
80. J. Larrea, M. B. Fontes, E. M. B.-Saitovitch, J. Plessel, M. M. Abd-Elmeguid, J. Ferstl, C. Geibel, A. Pereira, A. Jornada, M. A. Continentino, Phase diagram of the heavy fermion system $YbFe_2Ge_2$ under pressure. *Phys. Rev. B* **74**, 140406 (2006).
81. J. A. Hodges, Magnetic ordering of ytterbium in $YbCo_2Si_2$ and $YbFe_2Si_2$. *Europhysics Lett.* **4**, 749–753 (1987).
82. M. Francois, G. Venturini, J. F. Marêché, B. Malaman, B. Roques, De Nouvelles Séries de Germaniures, Isotypes de $U_4Re_7Si_6$, $ThCr_2Si_2$ et $CaBe_2Ge_2$, dans les Systèmes Ternaires R T Ge où R est un Elément des Terres Rares et T = Ru, Os, Rh, Ir: Supraconductivité de $LaIr_2Ge_2$. *J. Less Common Met.* **113**, 231–237 (1985).
83. H. Q. Yuan, M. Nicklas, Z. Hossain, C. Geibel, F. Steglich, Quantum phase transition in the heavy-fermion compound $YbIr_2Si_2$. *Phys. Rev. B* **74**, 212403 (2006).
84. J. Custers, P. Gegenwart, H. Wilhelm, K. Neumaier, Y. Tokiwa, O. Trovarelli, C. Geibel, F. Steglich, C. Pépin, P. Coleman, The break-up of heavy electrons at a quantum critical point. *Nature* **424**, 524–527 (2003).
85. O. Trovarelli, C. Geibel, M. Grosche, R. Schleser, R. Borth, G. Sparn, F. Steglich, Low-temperature properties of $YbCo_2Ge_2$. *Physica B Condens. Matter* **259-261**, 140–141 (1999).
86. M. Kolenda, A. Szytula, The valence state of Yb in $YbCo_2Si_2$ and $YbCo_2Ge_2$ compounds on the basis of magnetic susceptibility measurements. *J. Magn. Magn. Mater.* **79**, 57–60 (1989).
87. C. Klingner, C. Krellner, M. Brando, C. Geibel, F. Steglich, Magnetic behaviour of the intermetallic compound $YbCo_2Si_2$. *New J. Phys.* **13**, 083024 (2011).
88. Y. D. Seropegin, O. L. Borisenko, O. I. Bodak, V. N. Nikiforov, M. V. Kovachikova, Y. V. Kochetkov, Investigation of phase relationships and physical properties of Yb_2Pd_2Ge compounds. *J. Alloys Compd.* **216**, 259–263 (1995).
89. S. K. Dhar, E. V. Sampathkumaran, R. Vijayaraghavan, R. Kuentzler, $YbPd_2Si_2$, A moderate heavy fermion system. *Solid State Commun.* **61**, 479–481 (1987).
90. G. Knebel, D. Braithwaite, G. Lapertot, P. C. Canfield, J. Flouquet, Magnetically ordered Kondo lattice in $YbNi_2Ge_2$ at high pressure. *J. Phys. Condens. Matter* **13**, 10935–10946 (2001).
91. P. Bonville, J. A. Hodges, P. Imbert, G. Jéhanno, D. Jaccard, J. Sierro, Magnetic ordering and paramagnetic relaxation of $Yb3^+$ in $YbNi_2Si_2$. *J. Magn. Magn. Mater.* **97**, 178–186 (1991).
92. A. Grytsiv, D. Kaczorowski, V. H. Tran, A. Leithe-Jasper, P. Rogl, Crystal structure and physical properties of Yb-based intermetallics $Yb(Cu,Ag)_2(Si,Ge)_2$, $Yb(Cu_{1-x}Zn_x)_2Si_2$ (x = 0.65, 0.77) and $Yb(Ag_{0.18}Si_{0.82})_2$. *J. Alloys Compd.* **504**, 1–6 (2010).
93. J. Kaštil, M. Míšek, J. Kamarád, Z. Arnold, K. Vlášková, J. Prchal, M. Diviš, P. Doležal, J. Prokleška, J. Valenta, J. Fikáček, A. Rudajevová, D. Kriegner, Properties of the divalent-Yb compound $YbAu_2Si_2$ under extreme conditions. *Physica B Condens. Matter* **505**, 41–44 (2017).
94. A. Miyake, F. Honda, R. Settai, K. Shimizu, Y. Onuki, Development of the valence fluctuation in the nearly divalent compound $YbCu_2Ge_2$ under high pressure. *J. Physical Soc. Japan* **81**, SB054 (2012).
95. A. Fernandez-Pañella, V. Balédent, D. Braithwaite, L. Paolasini, R. Verbeni, G. Lapertot, J.-P. Rueff, Valence instability of $YbCu_2Si_2$ through its magnetic quantum critical point. *Physical Review B* **86**, 125104 (2012).
96. T. Nakano, M. Hedo, Y. Uwatoko, E. V. Sampathkumaran, High pressure effects on the electrical resistivity behavior of the Kondo lattice, $YbPd_2Si_2$. *Solid State Commun.* **132**, 325–328 (2004).
97. S. Lausberg, A. Hannaske, A. Steppke, L. Steinke, T. Gruner, L. Pedrero, C. Krellner, C. Klingner, M. Brando, C. Geibel, F. Steglich, Doped $YbRh_2Si_2$: Not only ferromagnetic correlations but ferromagnetic order. *Phys. Rev. Lett.* **110**, 256402 (2013).
98. J. A. Hodges, G. Jehanno, J. M. Friedt, Hyperfine interactions on ^{151}Eu and ^{57}Fe in amorphous $EuFe_2Si_2$. *Hyperfine Interact.* **27**, 365–368 (1986).
99. I. Nowik, I. Felner, Large crystalline fields and anisotropic vibrational modes of $^{151}Eu^{2+}$ in metallic $EuRu_2Ge_2$. *Physica B+C* **130**, 433–435 (1985).
100. A. Prasad, V. K. Anand, Z. Hossain, P. L. Paulose, C. Geibel, Anisotropic magnetic behavior in $EuIr_2Ge_2$single crystal. *J. Phys. Condens. Matter* **20**, 285217 (2008).
101. R. E. Gladyshevskii, E. Parthe, Crystal structure of europium dirhodium digermanium, $EuRh_2Ge_2$ with $ThCr_2Si_2$ type. *Z. Kristallogr.* **198**, 173–174 (1992).
102. A. Mitsuda, S. Hamano, N. Araoka, H. Yayama, H. Wada, Pressure-induced valence transition in antiferromagnet $EuRh_2Si_2$. *J. Physical Soc. Japan* **81**, 023709 (2012).
103. Y. Ashitomi, M. Kakihana, F. Honda, A. Nakamura, D. Aoki, Y. Uwatoko, M. Nakashima, Y. Amako, T. Takeuchi, T. Kida, T. Tahara, M. Hagiwara, Y. Haga, M. Hedo, T. Nakamah, Y. Ōnuki, Magnetic properties and effect of pressure on the electronic state of $EuCo_2Ge_2$. *Physica B Condens. Matter* **536**, 192–196 (2018).
104. S. Seiro, Y. Prots, K. Kummer, H. Rosner, R. C. Gil, C. Geibel, Charge, lattice and magnetism across the valence crossover in $EuIr_2Si_2$ single crystals. *J. Phys. Condens. Matter* **31**, 305602 (2019).
105. P. Maślankiewicz, J. Szade, Valence instability of europium in $EuCo_2Si_2$. *J. Alloys Compd.* **423**, 69–73 (2006).
106. T. Takeuchi, T. Yara, Y. Ashitomi, W. Iha, M. Kakihana, M. Nakashima, Y. Amako, F. Honda, Y. Homma, D. Aoki, Y. Uwatoko, T. Kida, T. Tahara, M. Hagiwara, Y. Haga, M. Hedo, T. Nakama, Y. Ōnuki, Effects of magnetic field and pressure on the valence-fluctuating antiferromagnetic compound $EuPt_2Si_2$. *J. Physical Soc. Japan* **87**, 074709 (2018).
107. E. V. Sampathkumaran, L. C. Gupta, R. Vijayaraghavan, K. V. Gopalakrishnan, R. G. Pillay, H. G. Devare, A new and unique Eu-based mixed valence system: $EuPd_2Si_2$. *J. Phys. C Solid State Phys.* **14**, L237–L241 (1981).
108. H. Wada, Y. Goki, A. Mitsuda, Transport properties of $EuNi_2Ge_2$ under high pressure. *J. Physical Soc. Japan* **87**, 034707 (2018).
109. R. Nagarajan, S. Patil, L. C. Gupta, R. Vijayaraghavan, ^{151}Eu Mössbauer studies in $EuNiSi_2$—A new mixed valence system—and in $EuNi_2Si_2$ and $EuNiSi_3$. *J. Magn. Magn. Mater.* **54–57**, 349–350 (1986).
110. I. Schellenberg, W. Hermes, S. Lidin, R. Pottgen, Structure and properties of the 5.5 K antiferromagnet $EuAu_2Ge_2$. *Z. Kristallogr.* **226**, 214–218 (2011).
111. H. -J. Hesse, G. Wortmann, ^{151}Eu-Mossbauer study of pressure induced valence transitions in EuM_2Ge_2 (M = Ni, Pd, Pt). *Hyperfine Interact.* **91**, 1499–1504 (1994).
112. E. R. Bauminger, I. Felner, D. Froindlich, D. Levron, I. Nowik, S. Ofer, R. Yanovsky, Mossbauer effect studies of interconfiguration fluctuations in metallics rare earth compounds. *J. Phys. Colloq.* **35**, C6–C70 (1974).
113. G. Bulk, W. Nolting, Antiferromagnetism in 4f-systems with valence instabilities. *Z. Physik B Condens. Matter* **70**, 473–483 (1988).
114. J. Gouchi, K. Miyake, W. Iha, M. Hedo, T. Nakama, Y. Onuki, Y. Uwatoko, Quantum criticality of valence transition for the unique electronic state of antiferromagnetic compound $EuCu_2Ge_2$. *J. Physical Soc. Japan* **89**, 053703 (2020).
115. B. C. Sales, R. Viswanathan, Demagnetization due to interconfiguration fluctuations in the RE-Cu_2Si_2 compounds. *J. Low Temp. Phys.* **23**, 449–467 (1976).
116. P. G. Pagliuso, J. L. Sarrao, J. D. Thompson, M. F. Hundley, M. S. Sercheli, R. R. Urbano, C. Rettori, Z. Fisk, S. B. Oseroff, Antiferromagnetic ordering of divalent Eu in $EuCu_2Si_2$ single crystals. *Phys. Rev. B* **63**, 092406 (2001).
117. W. H. Jiao, I. Felner, I. Nowik, G. H. Cao, $EuRu_2As_2$: A new ferromagnetic metal with collapsed $ThCr_2Si_2$-type structure. *J. Supercond. Nov. Magn.* **25**, 441–445 (2012).
118. T. Terashima, M. Kimata, H. Satsukawa, A. Harada, K. Hazama, S. Uji, H. S. Suzuki, T. Matsumoto, K. Murata, $EuFe_2As_2$ under high pressure: An antiferromagnetic bulk superconductor. *J. Physical Soc. Japan* **78**, 083701 (2009).
119. P. Proschek, J. Prchal, M. Diviš, J. Prokleška, K. Vlášková, J. Valenta, J. Zubáč, J. Kaštil, M. Hedo, T. Nakama, Y. Ōnuki, F. Honda, Weakly anisotropic ferromagnet $EuRu_2P_2$: Ambient and hydrostatic pressure characterization. *J. Alloys Compd.* **864**, 158753 (2021).
120. C. Feng, Z. Ren, S. Xu, S. Jiang, Z. Xu, G. Cao, I. Nowik, I. Felner, K. Matsubayashi, Y. Uwatoko, Magnetic ordering and dense Kondo behavior in $EuFe_2P_2$. *Phys. Rev. B* **82**, 094426 (2010).
121. Y. Singh, Y. Lee, B. N. Harmon, D. C. Johnston, Unusual magnetic, thermal, and transport behavior of single-crystalline $EuRh_2As_2$. *Phys. Rev. B* **79**, 220401 (2009).
122. M. Bishop, W. Uhoya, G. Tsoi, Y. K. Vohra, A. S. Sefat, B. C. Sales, Formation of collapsed tetragonal phase in $EuCo_2As_2$ under high pressure. *J. Phys. Condens. Matter* **22**, 425701 (2010).
123. M. Reehuis, W. Jeitschko, M. H. Möller, P. J. Brown, A neutron diffraction study of the magnetic structure of $EuCo_2P_2$. *J. Phys. Chem. Solid* **53**, 687–690 (1992).
124. D. Nakamura, M. Hedo, K. Uchima, Y. Takaesu, T. Nakama, K. Yagasaki, T. Fujiwara, T. Shigeoka, T. Matsumoto, Y. Uwatoko, Effects of pressure and magnetic field on transport properties of $EuCo_2P_2$. *J. Physical Soc. Japan* **3**, 011036 (2014).

125. G. Michels, M. Roepke, T. Niemöller, M. Chefki, M. M. Abd-Elmeguid, H. Micklitz, E. Holland-Moritz, W. Schlabitz, C. Huhnt, B. Buchner, A. Wurth, A. Mewis, V. Kataev, The anomalous valence state of Eu and magnetic order in $EuRh_2P_2$. *J. Phys. Condens. Matter* **8**, 4055–4062 (1996).
126. W. L. Nelson, A. S. Jayasinghe, D. Graf, S. Latturner, R. E. Baumbach, Electronic and magnetic properties of $EuNi_{2-\delta}Sb_2$ structural variants. *J. Phys. Condens. Matter* **32**, 315801 (2020).
127. V. K. Anand, D. C. Johnston, Physical properties of $EuPd_2As_2$ single crystals. *J. Phys. Condens. Matter* **26**, 286002 (2014).
128. G. Drachuk, A. E. Bohmer, S. L. Bud'ko, P. C. Canfield, Magnetization and transport properties of single crystalline RPd_2P_2 (R=Y, La-Nd, Sm-Ho, Yb). *J. Magn. Magn. Mater.* **417**, 420–433 (2016).
129. W. T. Jin, N. Qureshi, Z. Bukowski, Y. Xiao, S. Nandi, M. Babij, Z. Fu, Y. Su, T. Brückel, Spiral magnetic ordering of the Eu moments in $EuNi_2As_2$. *Phys. Rev. B* **99**, 014425 (2019).
130. Y. Hiranaka, A. Nakamura, M. Hedo, T. Takeuchi, A. Mori, Y. Hirose, K. Mitamura, K. Sugiyama, M. Hagiwara, T. Nakama, Y. Ōnuki, Heavy fermion state based on the Kondo effect in $EuNi_2P_2$. *J. Physical Soc. Japan* **82**, 083708 (2013).
131. S. Danzenbächer, D. V. Vyalikh, Y. Kucherenko, A. Kade, C. Laubschat, N. Caroca-Canales, C. Krellner, C. Geibel, A. V. Fedorov, D. S. Dessau, R. Follath, W. Eberhardt, S. L. Molodtsov, Hybridization phenomena in nearly-half-filled f-shell electron systems: Photoemission study of $EuNi_2P_2$. *Phys. Rev. Lett.* **102**, 026403 (2009).
132. K. Hiebl, C. Horvath, P. Rogl, M. J. Sienko, Magnetic properties and structural data of ternary silicides: (RE,Th,U)Os_2Si_2 (RE= rare earth). *Solid State Commun.* **48**, 211–215 (1983).
133. H. M. Duh, I. S. Lyubutin, I. M. Jiang, G. H. Hwang, K. D. Lain, Magnetic properties of $U(Pd_{1-x}Fe_x)_2Ge_2$. *J. Magn. Magn. Mater.* **153**, 86–96 (1996).
134. A. Szytuła, Ł. Gondek, M. Ślaski, B. Penc, A. Jezierski, Non-magnetic behaviour of UFe_2Si_2 compound. *J. Alloys Compd.* **442**, 275–278 (2007).
135. S. Süllow, G. J. Nieuwenhuys, A. A. Menovsky, J. A. Mydosh, S. A. M. Mentink, T. E. Mason, W. J. L. Buyers, Spin glass behavior in URh_2Ge_2. *Phys. Rev. Lett.* **78**, 354–357 (1997).
136. H. Ptasiewicz-Bak, Neutron diffraction study of magnetic ordering in UPd_2Si_2, UPd_2Ge_2, URh_2Si_2 and URh_2Ge_2. *J. Phys. F Met. Phys.* **11**, 1225–1235 (1981).
137. M. Kuznietz, H. Pinto, H. Ettedgui, M. Melamud, Neutron-diffraction study of the magnetic structure of UCo_2Ge_2. *Phys. Rev. B* **40**, 7328–7331 (1989).
138. T. Endstra, G. J. Nieuwenhuys, A. A. Menovsky, J. A. Mydosh, Structural and magnetic properties of UCo_2Ge_2. *J. Appl. Phys.* **69**, 4816–4818 (1991).
139. L. Chełmicki, J. Leciejewicz, A. Zygmunt, Magnetic properties of UT_2Si_2 and UT_2Ge_2 (T = Co, Ni, Cu) intermetallic systems. *J. Phys. Chem. Solid* **46**, 529–538 (1985).
140. M. Mihalik, A. Kolomiets, J. -C. Griveau, A. V. Andreev, V. Sechovsky, Magnetism of UCo_2Si_2 single crystal studied under applied magnetic field and hydrostatic pressure. *High Press. Res.* **26**, 479–483 (2007).
141. G. Quirion, F. S. Razavi, M. L. Plumer, J. D. Garrett, Pressure-temperature phase diagram of UPd_2Si_2 and UNi_2Si_2. *Phys. Rev. B* **57**, 5220–5224 (1998).
142. S. B. Roy, A. K. Pradhan, P. Chaddah, Magnetic properties of polycrystalline UNi_2Ge_2: Irreversibility and metastable behaviour. *J. Phys. Condens. Matter* **6**, 5155–5160 (1994).
143. C. Tabata, N. Miura, K. Uhlířová, M. Vališka, H. Saito, H. Hidaka, T. Yanagisawa, V. Sechovský, H. Amitsuka, Peculiar magnetism of UAu_2Si_2. *Phys. Rev. B* **94**, 214414 (2016).
144. T. D. Matsuda, S. Ikeda, E. Yamamoto, Y. Haga, Y. Onuki, Magnetic property of a single crystal UCu_2Ge_2. *J. Physical Soc. Japan* **76**, 074708 (2007).
145. T. D. Matsuda, Y. Haga, S. Ikeda, A. Galatanu, E. Yamamoto, H. Shishido, M. Yamada, J.-I. Yamaura, M. Hedo, Y. Uwatoko, T. Matsumoto, T. Tada, S. Noguchi, T. Sugimoto, K. Kuwahara, K. Iwasa, M. Kohgi, R. Settai, Y. Ōnuki, Electrical and magnetic properties of a single crystal UCu_2Si_2. *J. Physical Soc. Japan* **74**, 1552–1556 (2005).
146. Z. Fisk, N. O. Moreno, J. D. Thompson, Properties of Cu-flux-grown UCu_2Si_2. *J. Phys. Condens. Matter* **15**, S1917–S1921 (2003).
147. M. A. Avila, S. L. Bud'ko, P. C. Canfield, Anisotropic magnetization, specific heat and resistivity of RFe_2Ge_2 single crystals. *J. Magn. Magn. Mater.* **270**, 51–76 (2004).
148. I. Felner, J. Nowik, Magnetism and hyperfine interactions in EuM_2Ge_2 and GdM_2Ge_2 (M = Mn, Fe, Co, Ni, Cu). *J. Phys. Chem. Solid* **39**, 767–773 (1978).
149. A. Gallagher, K. W. Chen, C. M. Moir, S. K. Cary, F. Kametani, N. Kikugawa, D. Graf, T. E. Albrecht-Schmitt, S. C. Riggs, A. Shekhter, R. E. Baumbach, Unfolding the physics of URu_2Si_2 through silicon to phosphorus substitution. *Nat. Commun.* **7**, 10712 (2016).
150. Y. Dalichaouch, M. B. Maple, J. W. Chen, T. Kohara, C. Rossel, M. S. Torikachvili, A. L. Giorgi, Effect of transition-metal substitutions on competing electronic transitions in the heavy-electron compound URu_2Si_2. *Physica B Condens. Matter* **41**, 1829–1836 (1990).

Acknowledgments

Funding: R.E.B. acknowledges support from the National Science Foundation through NSF DMR-1904361. Y.L. was supported in part by the Center for Actinide Science and Technology, an Energy Frontier Research Center funded by the U.S. Department of Energy (DOE), Office of Science, Basic Energy Sciences (BES), under Award Number DE-SC0016568. J.Y.C. acknowledges NSF DMR-2209804 and Welch Grant number AT-2056-20210327 for partial support. The National High Magnetic Field Laboratory is supported by the National Science Foundation through NSF DMR-1644779 and the State of Florida. We acknowledge J. Ortega for drawing the crystal structures. We thank C. McNiel (NHMFL) for essential contributions in designing Figs. 3 to 6. **Author contributions:** R.E.B. conceived the project. All authors contributed equally to the compilation of data from the literature, its interpretation, and writing. J.Y.C. is primarily responsible for studies of composite structures that are referenced. **Competing interests:** The authors declare that they have no competing interests. **Data and materials availability:** All data needed to evaluate the conclusions in the paper are present in the paper and are available in the references.

Submitted 1 March 2022
Accepted 27 June 2022
Published 10 August 2022
10.1126/sciadv.abp8264